

NUMERICAL ANALYSIS OF TURBULENT FLOW WITH HEAT TRANSFER IN A SQUARE DUCT WITH 45 DEGREE RIBS

Yuria Okagaki
*Graduate School of
Engineering,
Utsunomiya University*
7-1-2 Yoto, Utsunomiya,
Tochigi, Japan 321-8585
Phone: +81-28-689-6032
okagaki.yuria@jaea.go.jp

Hitoshi Sugiyama
*Graduate School of
Engineering,
Utsunomiya University*
7-1-2 Yoto, Utsunomiya,
Tochigi, Japan 321-8585
Phone: +81-28-689-6031
sugiyama@cc.utsunomiya-u.ac.jp

Naoto Kato
*Graduate School of
Engineering,
Utsunomiya University*
7-1-2 Yoto, Utsunomiya,
Tochigi, Japan 321-8585
Phone: +81-28-689-6032
note@cc.utsunomiya-u.ac.jp

Atsuhiko Terada
Japan Atomic Energy Agency
4002, Narita-cho, Oarai-machi,
Higashiibaraki-gun, Ibaraki,
Japan 311-1393
Phone: +81-29-266-7664
terada.atsuhiko@jaea.go.jp

Ryutaro Hino
Japan Atomic Energy Agency
4002, Narita-cho, Oarai-machi,
Higashiibaraki-gun, Ibaraki,
Japan 311-1393
Phone: +81-29-266-7716
hino.ryutaro@jaea.go.jp

Keywords: Computational Fluid Dynamics, Heat Transfer, Algebraic Reynolds Stress Model, Turbulent Prandtl Number, Algebraic Turbulent Heat Flux Model, Heat Exchanger, HTGR

ABSTRACT

Turbulent flow and heat transfer characteristics in a square duct of 100 mm height with 45 degree square ribs of 10 mm height was analyzed numerically by using algebraic Reynolds stress model including the fixed turbulent Prandtl number and algebraic turbulent heat flux models.

In this research, analytical results were compared with the experimental and predicted data reported by Bonhoff et al. [1], which were measured and analyzed turbulent flow fields at Reynolds number 5×10^4 based on bulk velocity and duct height by means of a PIV system and a Reynolds stress model.

Analytical results obtained by algebraic Reynolds stress model showed a good agreement with the experimental data of streamwise and spanwise mean velocity profiles at the same Reynolds number of the experiment. As for secondary flow in the duct, analytical results showed relatively good agreement with the experimental data.

Moreover, temperature distributions were obtained by using the fixed turbulent Prandtl number and algebraic turbulent heat flux models. Temperature profiles of algebraic turbulent heat flux model were not similar to velocity profiles. Considering algebraic turbulent heat flux

model has potentiality to reproduce anisotropic temperature, these results suggested that correlation between momentum and heat transfer was not recognized in this turbulent field.

As a result of this study, it was verified that the presented method was able to predict turbulent flow in duct with ribs through the comparison of calculated results with the experimental data.

1. INTRODUCTION

Channels with periodic ribs have been used in many engineering fields due to its high heat transfer performance, and are expected for application of process heat exchange in nuclear heat application systems such as for hydrogen production using a high-temperature gas-cooled reactor (HTGR). To develop a design code of heat exchangers with ribs for HTGR heat application systems, as a first step, the one of effective methods of heat transfer enhancement is to arrange periodically ribs on duct wall [2]. This method produces actively the anisotropic turbulent flow and complicated flow near the heat transfer surface. When the anisotropic turbulence is produced, heat transfer performance is strongly affected by pattern changes of secondary flows having an effect on temperature fields.

Accurate prediction of the heat transfer performance depends on turbulent models. To improve prediction accuracy, many investigations have reported analytical studies on heat transfer enhancement by using periodically arranged ribs in ducts such as straight and U-shaped ducts, bend etc. Analytical studies are categorized as follows: heat transfer enhancement by the secondary flow of the second kind derived from anisotropic turbulent flow and that by the secondary flow of the first kind due to the pressure gradient force. In the latter case, while highly heat transfer enhancement is expected, pressure drop increases with heat transfer coefficients.

From the view point of compatible possibility with high heat transfer coefficients and rather low pressure drops, inclined ribs have been attracted. Han et al. [3], who determined the effect of rib angle of attack in a square duct with two opposite rib-roughened walls, demonstrated that the best thermal performance is achieved at a 30 and 45 degree angle to the flow for both the rib pitch to height ratios. He showed that the thermal performance was about 10-20 percent higher than the rib with a 90 degree angle to the flow, and the pumping power requirement for the angled rib was about 20-50 percent lower than the transverse rib. It takes it as given that a better performance than the ribs with a 90 degree angle to the flow which currently being used in the modern gas turbine internal cooling passages. Iacovides et al. [4] reported results of the measurement and numerical analysis in a square U-bend with inclined ribs of 45 degree. The measurement was performed by using laser-Doppler anemometry (LDA) in flow field, and the liquid crystal technique in temperature field. The numerical analysis was carried out by using high and low-Reynolds (Re) two equation models. Murata and Mochizuki [5] have examined numerically the effect of the angled rib on the flow and heat transfer by performing the large eddy simulation (LES) from the points of separation and reattachment caused by the angled ribs. These effects were clarified by making a comparison between the laminar and turbulent cases and also between angled 60 degree and transverse 90 degree rib cases. Jang et al. [6] presented calculated results for the turbulent flow and heat transfer for a two-pass square channel with and without 60 degree angled parallel ribs. They used the finite method, which solves the Reynolds-averaged Navier-Stokes equation in conjunction with a near-wall second-order Reynolds stress closure model, and a two-layer k- ϵ isotropic eddy viscosity model. Comparing the second-moment and two-layer calculations with the experimental data demonstrated that angled rib turbulators and the 180 degree sharp turn of the channel produced strong non-isotropic turbulence, which significantly affected the flow field and heat transfer coefficients. Bonhoff et al. [1] have performed experimental and numerical analysis of turbulent flow in a square duct with 45 degree ribs, and compared analytical results with the experimental data. Standard k- ϵ turbulent model with wall function method, a differential Reynolds stress model and a standard k- ϵ turbulence model with a two layer wall model has been adopted in prediction. Experimental data have measured by using particle image velocimetry (PIV) method.

To improve prediction accuracy of heat transfer

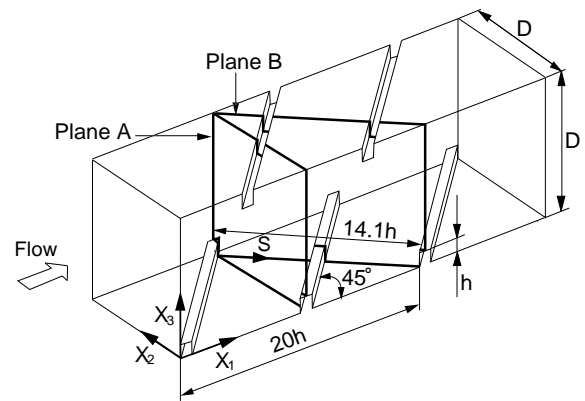


Fig. 1 Diagram of square duct with 45 degree ribs and definition of coordinate system

coefficients depending on turbulent models, availability of algebraic Reynolds stress model was verified with the experimental and analytical results by Bonhoff et al. [1]. This paper presents analytical results of flow and heat transfer characteristics in a square duct of 100 mm height with 45 degree square ribs of 10 mm height.

2. NOMENCLATURE

a	: thermal diffusivity
a_t	: turbulent thermal diffusivity
D	: side length of square cross-section
h	: rib height
P	: wall static pressure
p	: fluctuating pressure
T	: mean temperature
T'	: temperature fluctuation
T_w	: wall temperature
T_{in}	: mean temperature of internal cross-section
$\overline{u_i u_j}$: Reynolds stresses
$\overline{u_i T'}$: turbulent heat flux correlation
U_b	: cross-section mean velocity of square duct
$ U $: magnitude of velocity vectors $\sqrt{U_1^2 + U_2^2 + U_3^2}$
U_i	: i 'th mean velocity component
X_i	: i 'th Cartesian coordinate
δ_{ij}	: Kronecker delta
ν	: kinematics viscosity
ρ	: density
$(\)$: ensemble averaged value

3. NUMERICAL METHOD

3.1 Numerical Subject and Definition of Coordinate System

The duct configuration and coordinate system used in the calculation are shown in Fig. 1. The operating conditions correspond to those employed by Bonhoff et al. [1]. The ribs inclined 45 degree to streamwise velocity were located periodically on the top and bottom wall of the square duct. The duct with ribs cross-section of 10 mm \times 10 mm had a rectangular cross-section of 100 mm \times 100 mm. The Reynolds number was 5×10^4 based on the hydraulic diameter and the bulk velocity. The measuring Plane A and Plane B are

Table 1 Modeling of the pressure-strain correlation term

$\pi_{ij,1} + \pi_{ji,1}$	$-C_1 \frac{\varepsilon}{k} \left(\overline{u_i u_j} - \frac{2}{3} k \delta_{ij} \right)$
$\pi_{ij,2} + \pi_{ji,2}$	$-\frac{C_2 + 8}{11} \left(P_{ij} - \frac{2}{3} P_k \delta_{ij} \right) + \zeta k \left(\frac{\partial U_i}{\partial X_j} + \frac{\partial U_j}{\partial X_i} \right)$ $-\frac{8C_2 - 2}{11} \left(D_{ij} - \frac{2}{3} P_k \delta_{ij} \right)$
$[\pi_{ij} + \pi_{ji}]_w$	$C_1 = C_1^* + C_1' f \left(\frac{L}{X_w} \right) \quad C_2 = C_2^* + C_2' f \left(\frac{L}{X_w} \right)$ $\zeta_2 = \zeta_2^* + \zeta_2' f \left(\frac{L}{X_w} \right)$
$P_{ij} = -\overline{u_i u_j} \frac{\partial U_k}{\partial X_k} - \overline{u_j u_k} \frac{\partial U_i}{\partial X_k} \quad D_{ij} = -\overline{u_i u_k} \frac{\partial U_k}{\partial X_i} - \overline{u_j u_k} \frac{\partial U_k}{\partial X_j}$ $P_k = -\overline{u_k u_i} \frac{\partial U_k}{\partial X_i} \quad f \left(\frac{L}{x_w} \right) = \frac{C_\mu^{3/4} k^{3/2}}{\kappa \varepsilon X_w}$	

Table 2 Constants of the pressure-strain correlation term

C_1^*	C_2^*	ζ^*	C_1'	C_2'	ζ'	C_μ	κ
1.4	0.44	-0.16	-0.35	0.12	-0.1	0.09	0.42

perpendicular to the streamwise direction and the ribs, respectively. Bonhoff et al. [1] had measured fully developed turbulent flow by use of a PIV system. The coordinate system is defined as shown in Fig. 1. Spanwise direction is along the X_1 axis, the vertical direction is along the X_2 and the streamwise direction is along X_3 . The origin of the rectangular coordinate system is set at right-hand bottom of channel.

3.2 Governing Transport Equation

3.2.1 Flow field model

The Reynolds averaged Navier-Stokes equation (RANS) is expressed in the following form:

$$\frac{DU_i}{Dt} = -\frac{1}{\rho} \frac{\partial P}{\partial X_i} + \frac{\partial}{\partial X_j} \left[\nu \left(\frac{\partial U_i}{\partial X_j} + \frac{\partial U_j}{\partial X_i} \right) - \overline{u_i u_j} \right] \quad (1)$$

The Reynolds stresses that appear in the transport equation must be solved in order to obtain the velocity fields completely. In this calculation, we have adopted the transport equation of Reynolds stresses in order to accurately predict anisotropic turbulence. The transport equation of Reynolds stresses is displayed exactly in the following form:

$$\begin{aligned} \frac{D\overline{u_i u_j}}{Dt} = & - \left(\overline{u_i u_k} \frac{\partial U_j}{\partial X_k} + \overline{u_j u_k} \frac{\partial U_i}{\partial X_k} \right) + \frac{p}{\rho} \left(\frac{\partial u_i}{\partial X_j} + \frac{\partial u_j}{\partial X_i} \right) \\ & - \frac{\partial}{\partial X_k} \left\{ \overline{u_i u_j u_k} - \nu \frac{\partial \overline{u_i u_j}}{\partial X_k} + \frac{p}{\rho} (\delta_{jk} u_i + \delta_{ik} u_j) \right\} \\ & - 2\nu \frac{\partial \overline{u_i}}{\partial X_k} \frac{\partial \overline{u_j}}{\partial X_k} \end{aligned} \quad (2)$$

It is impossible to numerically solve the above equation directly, so it is necessary to rewrite several of the terms of the Reynolds stress equation by introducing the concept of the turbulent model. Moreover, with respect to the numerical analysis, the convection term of the left-hand side and the diffusion term of right-hand side of Eq. (2) make it difficult

Table 3 Modeling of the pressure-temperature gradient term

$\pi_{iT,1}$	$-C_{1T} \frac{\varepsilon}{k} \overline{u_i T'} - C_{1T}' \frac{\varepsilon}{k} \left(\overline{\frac{u_i u_j}{k}} - \frac{2}{3} \delta_{ij} \right) \overline{u_j T'}$
$\pi_{iT,2}$	$C_{2T} \overline{u_m T'} \frac{\partial U_i}{\partial X_m} - C_{2T}' \overline{u_m T'} \frac{\partial U_m}{\partial X_i}$
$\pi_{iT,w}$	$C_{1T} = C_{1T}^* \left\{ 1 + C_{1T,w} \cdot f \left(\frac{L}{X_w} \right) \right\}$ $C_{1T}' = C_{1T}'^* \left\{ 1 + C_{1T,w} \cdot f \left(\frac{L}{X_w} \right) \right\}$ $C_{2T} = C_{2T}^* \left\{ 1 + C_{2T,w} \cdot f \left(\frac{L}{X_w} \right) \right\}$ $C_{2T}' = C_{2T}'^* \left\{ 1 + C_{2T,w} \cdot f \left(\frac{L}{X_w} \right) \right\}$

Table 4 Constants of the pressure-temperature gradient term

C_{1T}^*	$C_{1T}'^*$	C_{2T}^*	$C_{2T}'^*$	$C_{1T,w}$	$C_{2T,w}$
3.9	-2.5	0.8	0.2	0.25	-0.46

to obtain a numerical solution because these terms require iterative calculations in order to obtain stable results. In the present study, these terms are modeled by adopting Rodi's [7] approximation. As a result of this approximation, these two terms are transformed into algebraic form from differencing form, and transport equation contributes to decrease in computational load. However, it is also true that interdependence of physical quantity disappears compared with differential equation. Pressure-stain correlation term plays an important role to distribute turbulent energy. The modeling process of pressure-stain correlation term is described in the other report [8] in detail. Tables 1 and 2 show the modeling of pressure-strain term and model constants, respectively.

3.2.2 Temperature field model

It is indispensable to predict turbulent heat fluxes in order to get precisely temperature profiles. From this point of view, the transport equation of the turbulent heat flux is adopted to realize anisotropic temperature. The transport equation of turbulent heat flux is expressed exactly as following form:

$$\begin{aligned} \frac{D\overline{u_i T'}}{Dt} = & - \left(\overline{u_i u_k} \frac{\partial T'}{\partial X_k} + \overline{u_k T'} \frac{\partial U_i}{\partial X_k} \right) \\ & - \frac{\partial}{\partial X_k} \left\{ \overline{u_i u_k T'} + \frac{P}{\rho} T' \delta_{ik} - \nu \frac{\partial \overline{u_i T'}}{\partial X_k} - a u_i \frac{\partial T'}{\partial X_k} \right\} \\ & + \frac{P}{\rho} \frac{\partial T'}{\partial X_i} - (\nu + a) \frac{\partial T'}{\partial X_k} \frac{\partial \overline{u_i}}{\partial X_k} \end{aligned} \quad (3)$$

where the terms on the right hand side represent the production of turbulent heat flux from the mean flow, the diffusion of turbulent heat flux, the pressure-temperature gradient effect which leads to inhomogeneity among the individual heat flux components, and its dissipation respectively. The convection and diffusion terms were modeled in a same manner to Rodi's [7] approximation for

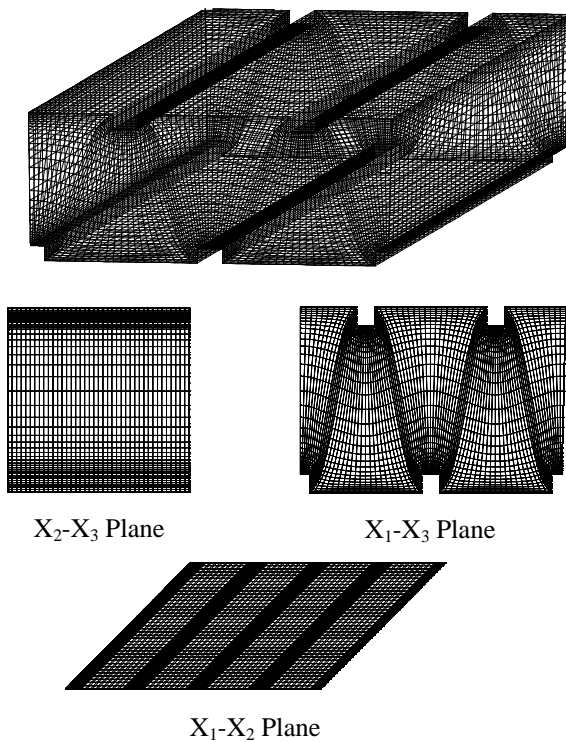


Fig. 2 Grids layouts for three dimensional view and cross sectional planes

Reynolds stress transport equation. By this approximation, the computational time can be saved. The pressure-temperature gradient term are composed of $\pi_{iT,1}$ and $\pi_{iT,2}$, which are called as slow and rapid return, respectively. The pressure-temperature gradient term is modeled as shown in Table 3. The model constants are listed in Table 4. Pressure-temperature gradient term $\pi_{iT,1}$ and $\pi_{iT,2}$ have been made use of concept presented by Lumley's [9] model and Launder's [10] model, respectively. Wall effect term $\pi_{iT,w}$ is modeled by introducing the function f . The function f has 1 near wall, and decreases as moving away from the wall. The derivation and the validity of the presented model have been described in a separate report [11] in detail.

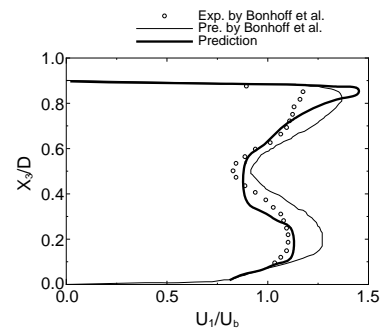
In addition to algebraic turbulent heat flux model, the simplest method, assuming that the turbulent Prandtl number is fixed, is adopted in this analysis. In this simplest model, turbulent heat flux is expressed as follows:

$$\overline{u_i T'} = a_t \frac{\partial T}{\partial X_i} \quad (4)$$

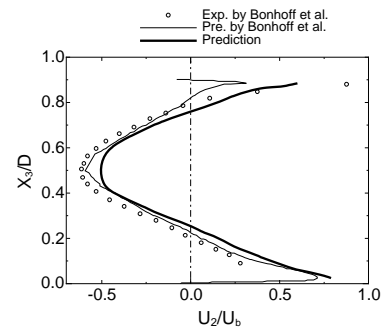
In this analysis, the turbulent Prandtl number is assumed to be 0.8. The calculated results of this method are compared with that of algebraic turbulent heat flux model to make model difference clear.

3.3 Numerical Analysis

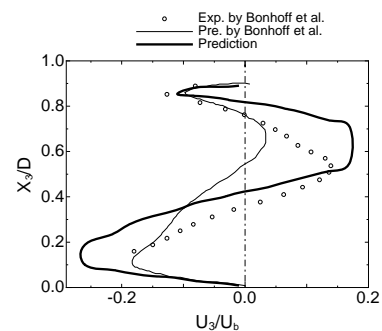
In the presented numerical analysis, the periodic boundary condition is applied to straight duct with two periodical spans. Therefore, exception for pressure, the values of inlet are set to be the same of outlet and, as for the pressure, the pressure gradient of inlet is equal to that of outlet. Figure 2 shows grid layouts. The number of computational grid points in the total



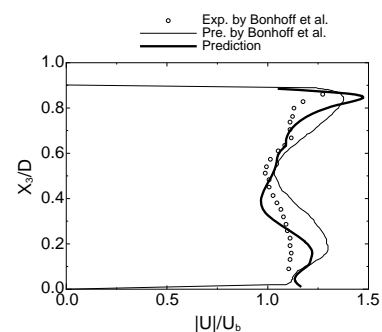
(a) Streamwise velocity



(b) Spanwise velocity



(c) Vertical velocity



(d) Velocity magnitude

Fig. 3 Comparison of velocity profiles

cross section is 41×31 , and 102 grid points are set along the streamwise direction. Therefore, the total number of computational grids is 129,642. The grids located near the wall are fine because the physical parameters changes rapidly near the wall. Since the presented turbulent model can be classified as a high-Reynolds-number turbulent model, the wall function method is used in the velocity field and the wall temperature is set to be constant as a boundary condition. The

buoyancy term is deleted from the momentum equation assuming that the buoyancy effect to the velocity field is negligible small. The governing equations were discretized by the differencing scheme, and QUICK (third-order upwind differencing scheme) was used for the convection term. Boundary-fitted coordinate system was used as a coordinate transformation method. In unsteady calculation with the explicit method, time step is determined to satisfy Courant number is kept under 1.

4. RESULTS AND DISCUSSION

4.1 Mean Velocity Field

Mean velocity profiles are compared with the experimental data measured by Bonhoff et al. [1] as shown in Fig. 3. It is noted that the calculated results of Reynolds stress model are displayed simultaneously with the presented result. In Fig. 3, symbol (a), (b) and (c) show the velocity profiles of streamwise, spanwise, and vertical direction, respectively. Symbol (d) shows the compared results of the three dimensional velocity vector magnitude profiles. The compared location is on line along X_3 axis at $X_2/D=0.5$ in Plane A as shown in Fig. 1.

In (a), the experimental distribution of the streamwise velocity exhibits the maximum value near the rib located the upper wall and small value in the central region of the channel. Besides, velocity profile indicates a peak value with approaching toward the lower wall. The calculated results can reproduce such characteristic phenomena. In (b), the experimental values show a positive value near the upper and lower walls and a negative value in the central region of the channel which means that circulating flow is generated. The experimental distribution of spanwise velocity rapidly increases as approaching near to the upper rib which also reproduces by algebraic Reynolds stress model, but minimum value is predicted more accurately by Reynolds stress model compared with algebraic Reynolds stress model. In (c), the experimental result shows that downstream flow is generated near the upper rib and the lower wall while upstream rapid velocity is produced in the central region of the channel. The two models can reproduce these characteristic profiles. However, two models fail to predict precisely the experimental profiles. In (d), this profile implies total prediction accuracy of the three directional velocities. Comparing the calculated results of the presented model with that of Bonhoff et al. [1], algebraic Reynolds stress model predicts the experimental value relatively well.

Figures 4 (a) and (b) show the comparison of secondary flow vectors and spanwise velocity profile in Plane A, respectively. From the top, the experimental and predicted results by Bonhoff et al. [1] and the presented results are indicated in the condition of setting viewpoint on downstream. In (a), the vector scale is not described in Bonhoff's paper, but it can be estimated from the experimental value of the spanwise velocity in Fig. 3. Its estimated vector scale was shown in this paper. However, the vector scale of calculated results by Bonhoff is unable to show because there is no description about the vector scale. From secondary flow vectors as shown in (a), it is clear that circulating flow near upper wall and counterclockwise circulating flow near lower wall are generated. Adding to this,

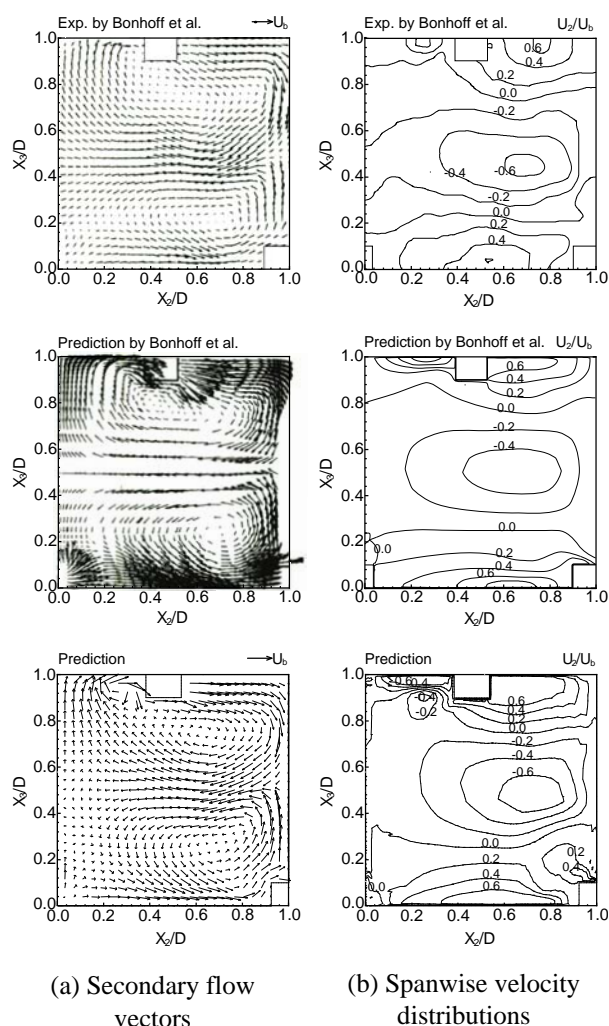


Fig. 4 Comparison of predicted and measured velocity profiles in Plane A

it is also pointed out as characteristic feature from the experiment that the secondary vector along $X_3/D=0.5$ moves wavy in the middle of cross section. In (b), the relatively large value formed near the upper and lower wall in the experimental result. This large velocity near upper and lower wall impinges on the side wall. As a result of this impingement, downward and upward flows are formed along side wall. These two flows are merged in the middle of side wall and its merged flow moves to the opposite side wall. The presented result reproduces these features and predicts well the value of -0.6 measured in the middle of cross section.

Figure 5 shows the compared result of the velocity vectors projected on Plane B. The projected velocity vectors are displayed as a bird's-eye figure which is vertically watching Plane B from upstream. The experimental results show only the velocity vectors around the rib, but the calculated results of Bonhoff et al. [1] show the projected velocity vectors in entire Plane B as well as the present calculated results. However, the velocity vector scale is not indicated in the figure because there is no information about vector scale in the paper presented by Bonhoff et al. [1]. In the experimental result, it is pointed out that the flow vectors near the rib located up stream show the incline upward flow from the rib

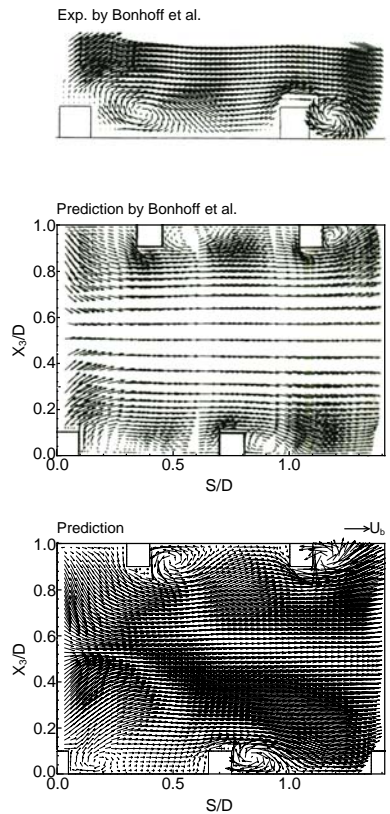


Fig. 5 Comparison of predicted and measured vectors in Plane B

corner to upper right and the circulating flow is recognized large area behind the rib. The calculated result by Bonhoff et al. [1] reproduces comparatively well this phenomenon. Although the presented calculation reproduces the incline upward flow, the size of the circulating flow behind the rib is smaller than the experiment. In addition, two models predict well reattachment point of separation behind the rib.

Judging from the comparison results of mean velocity filed, the experimental characteristic features can be reproduced by algebraic Reynolds stress model as well as Reynolds stress model. The difference between the two models is modeling of the convection and diffusion terms that expressed in differential form or in algebraic form. If two models can reproduce the experimental results, model validation depends on the production and pressure-strain correlation terms. Since it is not necessary to model the production term, the difference of the pressure-strain correlation term affects to the numerical solution. In case of the Reynolds stress model used by Bonhoff et al. [1] which is commercial numerical code, the pressure-stain correlation term isn't described in detail in their paper. In general, the secondary flow of the second kind depends greatly on the pressure-stain correlation term modeling in anisotropic turbulent flow. It has been already confirmed that the algebraic Reynolds stress model used in the presented analysis can reproduce the secondary flow of the second kind [12].

Figure 6 shows the comparison results of six Reynolds stress components formed in cross-section of Plane A. Reynolds stresses $\overline{u_1^2}$, $\overline{u_2^2}$, and $\overline{u_3^2}$ are normal stresses for streamwise, spanwise, and vertical, respectively. Reynolds stresses $\overline{u_1u_2}$, $\overline{u_1u_3}$, and $\overline{u_2u_3}$ are shear stress. In turbulence

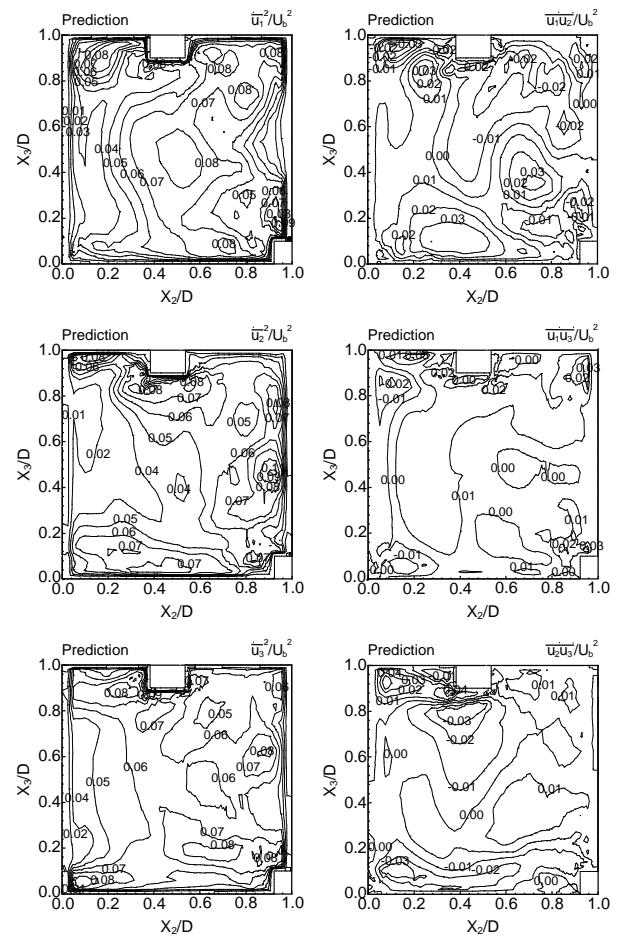


Fig. 6 Comparison of predicted distribution of normal and shear stresses in Plane A

of square duct without rib, the normal stress for streamwise displays the highest value compared with the other normal stress. By contrast, calculated results show that all normal stresses indicate high value near the rib and generate actively turbulence, which are considered as a characteristic distribution for turbulent flow in straight duct with the inclined ribs. On the other hand, about the share stress, in the case of turbulent filed of square duct without rib, shear stress $\overline{u_2u_3}$ is small absolute value, but shear stress $\overline{u_2u_3}$ of this case is large absolute value which are the same value of other share stresses. These results suggest that momentum transfer was performed actively in three directions by setting inclined rib.

4.2 Mean Temperature Field

Figures 7 and 8 show the streamwise velocity distribution and the temperature distribution in Plane A, respectively. Symbol (a), (b) in Fig. 8 are calculated contour maps of the fixed turbulent Prandtl number model and algebraic turbulent heat flux model, respectively.

In the case of the fixed turbulent Prandtl number model, Fig. 8 (a) suggest that there is a correlation between heat transfer and momentum transfer, judging from that temperature distribution is similar to streamwise velocity distribution which is shown in Fig. 7. By contrast, the contour map in Fig. 8 (b) is not similar to streamwise velocity distribution. Considering the algebraic turbulent heat flux

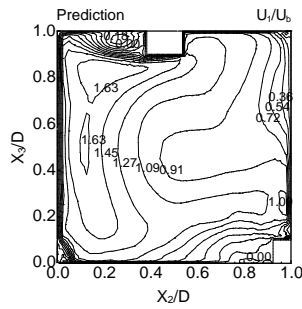


Fig. 7 Predicted streamwise velocity distribution in Plane A

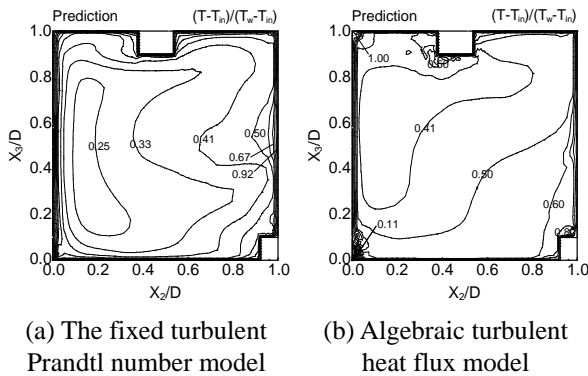


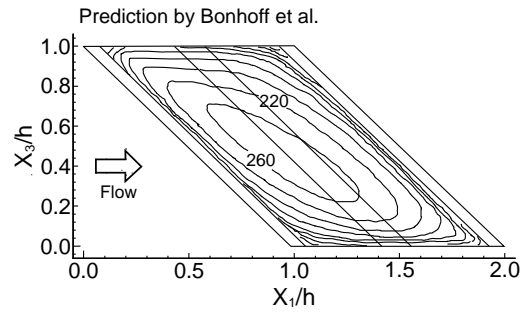
Fig. 8 Comparison of predicted distribution of temperature in Plane A

model has potentiality to predict anisotropic temperature field, it is concluded that the correlation between heat transfer and momentum transfer is not realized in this turbulent flow with inclined ribs.

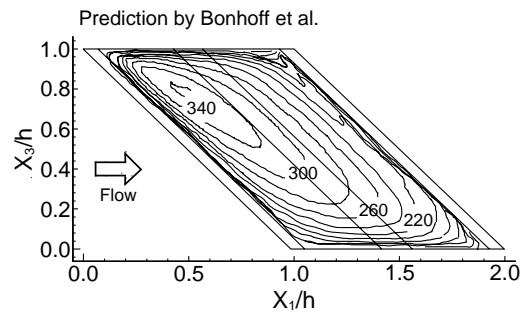
Figure 9 shows the compared results of distribution for Nusselt number over lower wall. Bonhoff et al. [1] predicted temperature field by using results of (a) Reynolds stress model and (b) $k-\epsilon$ model. The method for analyzing temperature field isn't described in detail in their paper. On the other hand, the presented results was predicted temperature field by (c) the fixed turbulent Prandtl number model and (d) algebraic turbulent heat flux model by using the velocity field solved by algebraic Reynolds stress model. In (a), the area of high heat transfer is formed in the middle of bottom wall, while, in (b), high Nusselt number is recognized just near downstream of the rib. About the phenomenon of (b), Bonhoff et al. [1] pointed out that the location of high Nusselt number corresponds to the location of reattachment point in Plane B which feature is related with the secondary flow. Both results of (c) and (d) show high Nusselt number is also formed in the same area of (b). Besides, It is found in figure (d) that the second highest area is generated in the center of bottom wall which means algebraic turbulent heat flux model predict high value of Nusselt number not only near just downstream behind rib but also center of bottom wall.

5. CONCLUSIONS

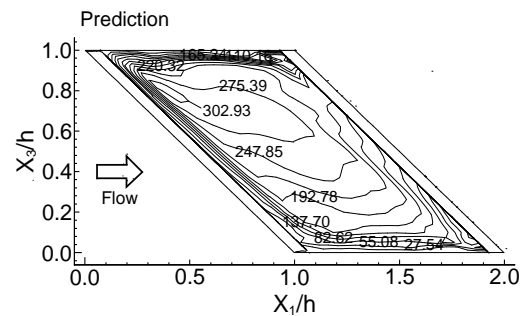
A numerical analysis has been performed for turbulent flow with heat transfer in a square duct with 45 degree ribs by using the algebraic Reynolds stress, the fixed turbulent



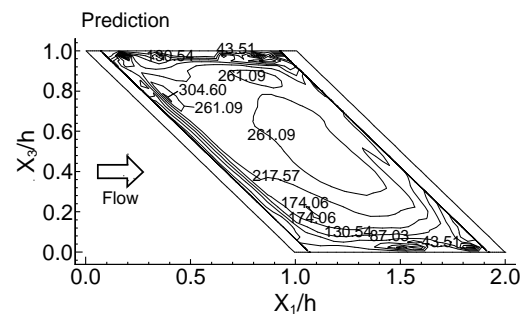
(a) Reynolds stress model



(b) $k-\epsilon$ model



(c) The fixed turbulent Prandtl number model



(d) Algebraic turbulent heat flux model

Fig. 9 Comparison of predicted distribution of Nusselt number

Prandtl number, and the algebraic turbulent heat flux models. Analytical results were compared with the experimental and predicted data reported by Bonhoff et al. [1] in order to confirm the validity of the presented models. As results of this analysis, the following conclusions are summarized:

- (1) The presented method was able to predict three directional velocities except for vertical velocity, which tendency was the same as that obtained with the Reynolds stress model. Although the agreement with

the experimental results were not perfect, characteristic features are realized by the algebraic Reynolds stress model.

- (2) The algebraic Reynolds stress relatively well reproduces the streamwise flow, the vector pattern and the reattachment point in Plane B as well as those obtained with the Reynolds stress model. The algebraic Reynolds stress model can predict anisotropic turbulent flow in duct with 45 degree ribs to present six Reynolds stresses.
- (3) The temperature contour map obtained by the algebraic turbulent heat flux model was not similar to velocity contour map. Since the algebraic turbulent heat flux model has potentiality to reproduce anisotropic temperature, correlation between momentum and heat transfer was not organized in this kind of turbulent field.
- (4) The fixed turbulent Prandtl number and algebraic turbulent heat flux models predicted similar values of Nusselt number.

Roughened Wall by Means of Algebraic Heat Flux Models”, *Int. J. Heat and Fluid Flow*, **23**(1), pp. 13-21.

- [12] Sugiyama, H., et al., 2006, “Numerical Analysis of Developing Turbulent Flow in a Rectangular Duct with Abrupt Change from Rough to Smooth Wall”, *Trans. JSAE*, **37**(2), pp. 97-102 [in Japanese].

REFERENCES

- [1] Bonhoff, B., et al., 1999, “Experimental Numerical Study of Developed Flow and Heat Transfer in Coolant Channels with 45 degree Ribs”, *Int. J. Heat and Fluid Flow*, **20**(3), pp. 311-319.
- [2] Sanokawa, K., et al., 1999, “Thermal and Fluid-dynamic Research and Development for High Temperature Gas Cooled Reactor in JAERI”, *JAERI-Review*, 98-024, pp. 112-135 [in Japanese].
- [3] Han, J. C., et al., 1985, “Heat Transfer Enhancement in Channels with Turbulence Promoters”, the *ASME, J. Eng. Gas Turbines and Power*, **107**(3), pp. 628-635.
- [4] Iacovides, H., et al., 2003, “Flow and Heat Transfer in Straight Cooling Passages with Inclined Ribs on Opposite Walls: an Experimental and Computational Study”, *Exp. Therm. Fluid Sci.*, **27**(3), pp. 283-294.
- [5] Murata, A., and Mochizuki, S., 2001, “Comparison between Laminar and Turbulent Heat Transfer in a Stationary Square Duct with Transverse or Angled Rib Turbulators”, *Int. J. Heat and Mass Trans.*, **44**(14), pp. 1127-1141.
- [6] Jang, Y-J., et al., 2001, “Computation of Flow and Heat Transfer in Two-Pass Channels with 60 deg Ribs”, *Trans. ASME J. Heat Transfer*, **123**(3), pp. 563-575.
- [7] Rodi, W., 1976, “A new algebraic relation for calculation the Reynolds stresses”, *Z. Angew. Math. Mech.*, **56**, pp. 219-221.
- [8] Sugiyama, H., and Hitomi, D., 2005, “Numerical analysis of developing turbulent flow in a 180° bend tube by algebraic Reynolds stress model”, *Int. J. Numer. Meth. Fluids*, **47**(12), pp. 1431-1449.
- [9] Lumley, J. L., 1975, “Introduction in Prediction Methods for Turbulent Flows”, *Lecture Series*, **76**, von Karman Inst., Belgium.
- [10] Launder, B. E., 1975, “Progress in The Modeling of Turbulent Transport”, *Lecture Series*, **76**, von Karman Inst., Belgium.
- [11] Sugiyama, H., et al., 2002, “Calculation of Turbulent Heat Flux Distributions in a Square Duct with One